A comparison of q-ball and PASMRI on sparse diffusion MRI data

D. Alexander[1]

[1]Computer Science, University College London, London, United Kingdom

Introduction. Recent studies [1-7] have highlighted the failure of diffusion tensor MRI in regions of complex microstructure such as white-matter fibre-crossings. Diffusion tensor MRI adopts a Gaussian model of the displacement density function p, which fits the data poorly in regions of fibre-crossings. Several alternative approaches can resolve the orientations of crossing fibres. A simple approach is the diffusion spectrum imaging (DSI) method of Wedeen et al [3], which acquires measurements on a grid of wavenumbers $\boldsymbol{q}$ allowing fast Fourier transform reconstruction of p. This technique requires long acquisition times to provide sufficient detail in p. However, DSI is wasteful of information, as only the angular structure of the reconstructed p provides information about fibre orientations and the radial component is typically discarded. Recent techniques reconstruct only the angular structure of p from measurements spread over a shell of wavenumbers with fixed $|\boldsymbol{q}|$. Tuch's q-ball algorithm [4] estimates the orientation distribution function $\varphi(p)$, which is the feature determined in DSI. Jansons and Alexander's PASMRI algorithm [5] extracts the persistent angular structure (PAS) of p. Both $\varphi(p)$ and the PAS are functions of the unit sphere and their peaks provide estimates of fibre orientations. Tuch tests q-ball on data sets with 492 measurements per voxel acquired with $|\boldsymbol{q}|=3.6\times10^5$ m^{-1} ($b \approx 4000$ s mm^{-2}). The estimates of φ closely resemble those from DSI. Jansons and Alexander show in simulation that PASMRI recovers the directions of two or three orthogonal crossing fibres from sparser data sets with 54 measurements acquired with $|\boldsymbol{q}|=2.0\times10^5$ m^{-1} ($b \approx 1200$ s mm^{-2}), which is more typical of clinical diffusion MRI. Here we compare the abilities of these two methods to recover crossing fibre directions from sparse data with relatively low $|\boldsymbol{q}|$, as used in [5], and compare performance in simulation as we vary some properties of the data.

Methods. The brain data set used in this study is a 128×128×60 array of voxels reconstructed from a 62×96×60 measurement array. Each voxel contains $M = 6$ measurements with $\boldsymbol{q} = \boldsymbol{0}$ and $N = 54$ measurements with unique gradient directions and $|\boldsymbol{q}| = Q = 2.0\times10^5$ m^{-1}. The gradient directions minimize the electrostatic energy of N pairs of equal and opposite points on the unit sphere with equal charges. The gradient pulse separation $\Delta = 0.04$ s; the gradient pulse duration $\delta = 0.034$ s; the magnitude of the gradients $|\boldsymbol{g}| = 0.022$ T m^{-1}. The average signal to noise ratio in the $\boldsymbol{q} = \boldsymbol{0}$ images $S \approx 16$ in white matter regions.

We synthesize data by emulating the scanner sequence. Given a model p for the diffusion displacement density, we sample F, the Fourier transform of p, M times at $\boldsymbol{q}=\boldsymbol{0}$ and once at each non-zero wavenumber sampled by the scanner. To each sample we add a random complex number with independent real and imaginary parts each with distribution N(0, σ^2), where $\sigma = F(0)/S$. The modulus of the noisy sample is the synthetic measurement. We use variations of three basic test functions:

$p_1(x) = G(x; \mathsf{D}_1, t)$,

$p_3(x) = (G(x; \mathsf{D}_1, t) + G(x; \mathsf{D}_2, t))/2$, and

$p_4(x) = (G(x; \mathsf{D}_1, t) + G(x; \mathsf{D}_2, t) + G(x; \mathsf{D}_3, t))/3$,

where $G(.; \mathsf{D}, t)$ is a zero-mean trivariate Gaussian function with covariance matrix $2t\mathsf{D}$ and t is the diffusion time; the diffusion tensors are $\mathsf{D}_1 = \mathrm{diag}(\lambda_1, \lambda_2, \lambda_2)$, $\mathsf{D}_2 = \mathrm{diag}(\lambda_2, \lambda_1, \lambda_2)$, $\mathsf{D}_3 = \mathrm{diag}(\lambda_2, \lambda_2, \lambda_1)$; $\lambda_1 = 17\times10^{-10}$ m^2 s^{-1} and $\lambda_2 = (21\times10^{-10} - \lambda_1)/2$.

To determine the ability of a method to recover directions from the test functions, we compute a performance index called the consistency fraction C. We use PASMRI and q-ball to estimate the principal directions of p from noisy synthetic data. The result is *consistent* if the number of estimated directions equals the number of ridges of p and the estimated directions match the ridge directions of p to within a small angular tolerance, which we set to $\cos^{-1}(0.95)$. The consistency fraction is the fraction of 256 trials in which the result is consistent.

Both PASMRI and q-ball contain parameters that must be tuned to maximize performance. The PASMRI algorithm has a regularization parameter r and a search radius ρ in the algorithm to find local maxima of the PAS. The q-ball algorithm has several regularization parameters and a similar search radius. We select values of these parameters that maximize the sum of the consistency fractions for p_1, p_3 and p_4 using the scanning sequence of the brain data over a discrete grid of possible settings.

Experiments and Results. Figure 1 shows principal directions maps over part of a coronal slice through the pons and the corpus callosum for PASMRI (bottom-left) and q-ball (bottom-right). The characteristic reduction in anisotropy in the fibre crossing at the pons is clear in the anisotropy map (top). In the pons, PASMRI extracts the expected left-right and superior-inferior fibre directions of the intersecting cortico-spinal tract and trans-pontine fibres consistently in the region of the pons. The q-ball algorithm only recovers both directions in about half the voxels in the pons region. Both algorithms recover single fibre directions consistently in the corpus callosum and cortico-spinal tract outside the fibre crossing.

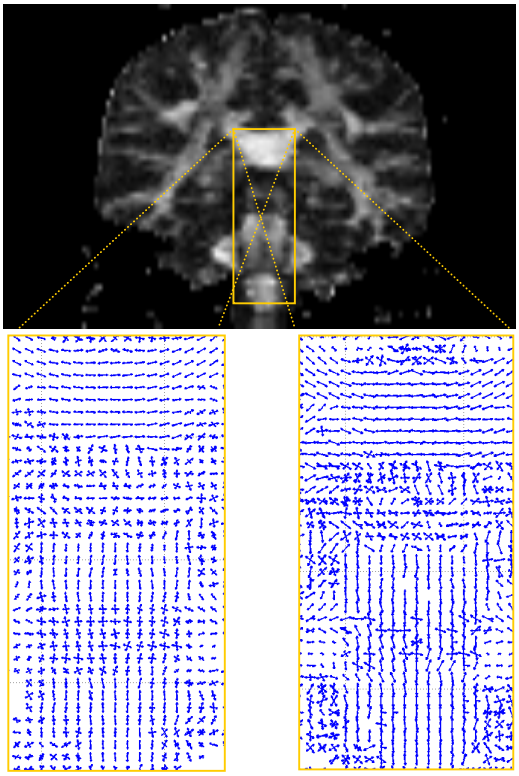

Figure 1. Shows the principal directions from PASMRI (left) and q-ball (right) in the pons and corpus callosum.

Figure 2 shows a plot of C against S for each test function using both algorithms. As expected, C increases with S. For p_3 and p_4, C increases more quickly for PASMRI that q-ball; for p_1, C increases more quickly using q-ball. Using PASMRI, $C > 95\%$ for p_1, p_3 and p_4 with $S > 16$ and using q-ball only with $S > 24$. Other experiments with synthetic data show that: 1) reducing λ_1 reduces C more quickly using PASMRI for p_1, but more quickly using q-ball for p_3 and p_4. 2) For all the test functions, increasing $|\boldsymbol{q}|$ increases C with both algorithms to a peak at approximately $2Q$. 3) For p_1, $C > 95\%$ with $N \geq 10$ using PASMRI, $N \geq 20$ using q-ball; for p_3, $C > 95\%$ with $N \geq 20$ using PASMRI, $N \geq 40$ using q-ball; for p_4, $C > 95\%$ with $N \geq 54$ using PASMRI, $N \geq 110$ using q-ball.

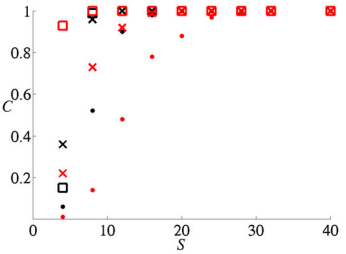

Figure 2. Plots C against S for p_1 (□), p_3 (×) and p_4 (•) using PASMRI (black) and q-ball (red).

Conclusion. The PASMRI algorithm appears more sensitive to directions in the data and gives cleaner principal direction maps on current data sets. However, results on synthetic data suggest that q-ball can achieve similar performance with a moderate increase in data quality. The q-ball algorithm is faster than PASMRI by several orders of magnitude, so the investment in higher quality data will often be justified. Computation times in PASMRI may be reduced in alternative implementations of the algorithm to that presented [5], though it is not clear how this will affect performance. Possible improvements to the q-ball algorithm may increase performance. Similar algorithms presented in [6] and [7] will be compared. We note that other indices of performance must be considered in a full performance comparison, such as accuracy and consistency of indices of shape derived from these algorithms. These will be examined in future work.

References. 1. L.R. Frank. *Magn. Reson. Med.*, 47, 1083, 2002. 2. D.C. Alexander, *et al.*, *Magn. Reson. Med.*, 48, 331, 2002. 3. Wedeen, *Proc. 7th ISMRM*, 321, 2000. 4. D.S. Tuch, PhD Thesis, MIT 2002. 5. K.M. Jansons and D.C. Alexander, *Inverse Problems*, 19, 1031, 2003. 6. C. Lin et al. , *Proc 11th ISMRM*, 2120, 2003. 7. A. Anderson and Z. Ding, *Proc. 10th ISMRM*, 440, 2002.

Acknowledgements. Dr Claudia Wheeler-Kingshott of the Institute of Neurology, UCL, provided the brain data used in this work.